Geophys. J. Int. (2003) **152,** 353–371

Depth imaging of basalt flows in the Faeroe–Shetland Basin

Moritz M. Fliedner* and Robert S. White

Bullard Laboratories, University of Cambridge, Madingley Road, Cambridge, UK. E-mail: rwhite@esc.cam.ac.uk

Accepted 2002 August 6. Received 2002 July 29; in original form 2001 November 23

SUMMARY

We use a grid of long-offset seismic profiles to map the thickness of subsurface basalt flows that extend southeastward across the Faeroe Shelf. Offsets of up to 38 000 m were achieved using two seismic acquisition vessels towing multichannel streamers and shooting alternately. Wide-angle reflections and refractions from the basalt and underlying strata allow us to build a velocity model down to the basement Lewisian crust. The velocity models give a first-order picture of the geology of low-velocity sediments of presumed early Palaeocene and Mesozoic age beneath the basalt flows. They also provide a control for pre-stack depth migration of the entire seismic data set, thus allowing us to produce good depth images of the structure. Pre-stack depth migration of selected wide-angle arrivals, such as those from the base of the basalt and the underlying basement, produce strong reflection images that allow these interfaces to be identified unambiguously on the higher-resolution images produced from the entire data set: in particular, we can distinguish between the primary and multiple reflections. We thus use the very long-offset arrivals to 'tag' the velocities of the geological interfaces from which they are returned, and hence to improve both the imaging and the interpretation of the basalt flows and the underlying structure.

Key words: Faeroe–Shetland Basin, long-offset seismic, rifting, subbasalt imaging, synthetic aperture profiling.

INTRODUCTION

Breakup of the northern North Atlantic in the early Tertiary was accompanied by massive production of molten rock, some of which was extruded as large basalt flows and the rest of which was intruded or underplated as sills in the crust. An estimated 10^6 km^3 of basalts were extruded within a period of 1–3 Myr (White & Mckenzie 1989; Saunders *et al.* 1997). The molten rock was generated by decompression of mantle as it rose beneath the zone of lithospheric thinning that subsequently broke to form the margins of the new North Atlantic Ocean. The unusually large volumes of melt were generated because the mantle was 150–200 °C hotter than normal because of the presence of the Iceland mantle plume (White & Mckenzie 1989; Barton & White 1997a).

The majority of the basaltic rock accumulated within and immediately adjacent to the rift zone, above where it was formed in the mantle. The pile of extrusive lavas reaches more than 7 km thick on the Faeroe Islands (Richardson *et al.* 1998), which lay above the hottest part of the mantle thermal anomaly at the time of breakup. Where there were prominent normal fault blocks caused by extension in the rift zone, the lavas initially ponded in the lows between the fault blocks; this can be seen on seismic reflection data from both the Rockall and the Greenland continental margins (Barton & White 1997b; Larsen *et al.* 1998). The extrusive lavas imaged on seismic reflection profiles have been drilled on the continental margins on both sides of the ocean, and at several locations along both margins, including the Vøring margin (Eldholm *et al.* 1989), the Rockall continental margin (Roberts *et al.* 1984), the Faeroe Islands (Berthelsen *et al.* 1984; Kiørboe & Petersen 1995), and the East Greenland margin (Saunders *et al.* 1998; Larsen *et al.* 1999a).

The seaward end of the flows, where they are thickest, subsequently subsided owing both to the weight of the lava pile itself and to thermal relaxation and subsidence of the underlying thinned lithosphere. This subsidence formed seaward-dipping reflection sequences that are readily recognized on seismic reflection profiles around the North Atlantic margins (Hinz 1981; Mutter & Zehnder 1988; Larsen & Jakobsdóttir 1988; Planke & Eldholm 1994; Barton & White 1997b).

Such was the rate of melt production in the rift zone that once the local topography of the rifted region had been filled by basalt, subsequent lavas were able to flow long distances away from the rift. They probably flowed on to the continental hinterland on both sides of the rift, but in the case of the North Atlantic, the western side now lies beneath the thick ice cover of the Greenland ice cap, so the extent of lava flows there is difficult to assess. Nevertheless, petrologic studies show that basaltic lavas of the same composition are found in both the Faeroe Islands and in Greenland (Larsen *et al.* 1999b), so they probably came from the same central source.

Where the palaeotopography adjacent to the rift was either flat-lying or formed by gently dipping sediments, the lavas were able

*Now at: 3DGeo Development Inc., Mountain View, CA, USA.

to flow long distances uninterrupted by topographic barriers. Such was the case in the Palaeogene east of the Faeroe Islands, and thick lava flows extend 150 km away from the islands over the earliest Tertiary sediments. The source region of the basalt flows, which was on the rifted margin west of the present Faeroe Islands was elevated above sea level at the time of rifting by the presence of the underlying anomalously hot mantle, and by crustal thickening caused by igneous underplating (Barton & White 1997a). The palaeotopography sloped gently down towards the older Mesozoic rifts of the Faeroe–Shetland Channel, and the basaltic lavas flowed downhill over these sediments away from the islands. Marked escarpments in the lava flows north and east of the present Faeroe Islands delineate the location of former coastlines at the time (Smythe 1983; Andersen 1988; Kiørboe 1999).

The feather edge of the lava flows (marked by a dotted line in Fig. 1) is reached some 150 km southeast of the Faeroe Islands (Stoker *et al.* 1993). On the Faeroe shelf the basalt flows thin from over 3000 m immediately east of the Faeroe Islands to zero in the Faeroe–Shetland Trough (Richardson *et al.* 1999; Smallwood *et al.* 2001). The furthest eastward subsurface sampling of the basalt flows is a thin section drilled in hole 205/9-1 (Fig. 1) of subaerial Faeroes lavas from the Upper Basalt Series (probably 56–55 Ma) within the Flett Formation (Ritchie *et al.* 1999). The basalt flows overlie the thick earliest Tertiary and Mesozoic sediments accumulated in

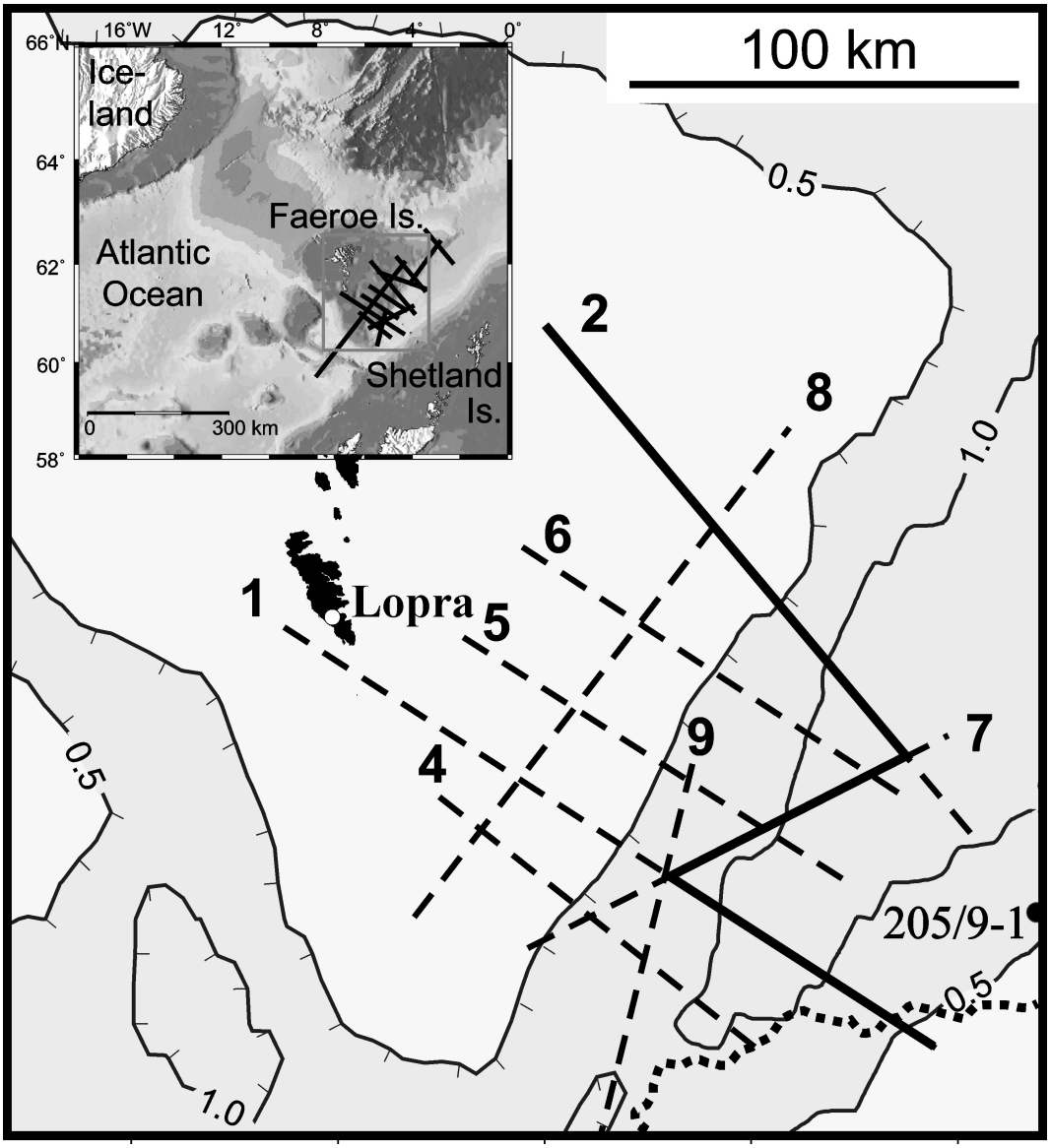

Figure 1. Map showing the location of long-offset two-ship profiles of the FLARE project used in this paper. The dotted line marks southeastern limit of Tertiary basalt flows (Stoker *et al.* 1993). Bathymetric contours are in kilometres. Profiles 1 and 2 used three passes of the two ships to achieve maximum offsets of 38 000 m (White *et al.* 1999), profiles 4–9 used a single pass with two ships to record maximum offsets of 18 000 m. The solid heavy line marks the location of the composite seismic profile in Fig. 15. The inset shows the location of the survey area on the northwest European continental margin, and highlights the extent of the 30–35 km thick igneous crust of the Iceland–Faeroe Ridge formed above the Iceland mantle plume as the North Atlantic opened; solid lines mark location of all 12 FLARE profiles. The onshore Lopra borehole (which penetrated the Lower Basalt Series) and offshore hole 205/9-1 (which penetrated the Upper Basalt Series) are shown by circles.

basins formed by earlier episodes of stretching of the continental lithosphere during the period extending from the late Carboniferous through to the early Palaeocene (Duindam & Van Hoorn 1987; Earle *et al.* 1989; Turner & Scrutton 1993). Pre-Tertiary sediment thicknesses reach a maximum of 8 km in the Faeroe–Shetland Basin (Stoker *et al.* 1993), and thin towards the present Faeroe Islands.

In this paper we use a grid of long-offset two-ship seismic profiles over the Faeroe shelf (Fig. 1) acquired in the Faeroe Large Aperture Research Experiment (FLARE) to image the thickness of the basalt flows as they extend away from the Faeroe Islands, and to constrain the thickness of underlying sediments above the deeper Palaeozoic and older crustal basement. The deep basement across the entire region between the Shetland and the Faeroe Islands is probably Lewisian gneiss that formed the foreland for the Caledonian orogeny (Stoker *et al.* 1993). However, other Caledonian terranes are probably juxtaposed against the Lewisian. At least between Orkney and Shetland the Lewisian is overlain by Moine and Devonian rocks, and adjacent to the northwest corner of the Scottish mainland by Torridonian and Cambro-Ordovician sediments. The seismic profiles described in this paper do not resolve this deep crustal structure, although it forms a high-velocity seismic basement across the entire region.

The episodic extension that has affected the Faeroe–Shetland region since the late Carboniferous or early Permian created a series of half-grabens, which filled with younger sediments. The sediments themselves have subsequently become indurated, so may also form a high-velocity 'seismic basement' on our profiles. To the east of our survey area, in the portion of the Faeroe–Shetland Trough not covered by basalt flows, these syntectonic grabens can be seen on seismic reflection profiles to have accumulated sediment wedges up to 8000 m thick against the basin-bounding faults (Stoker *et al.* 1993).

In the early Palaeocene, sedimentation in the Faeroes–Shetland Basin was controlled by the underlying end-Cretaceous fault-induced topography (Ebdon *et al.* 1995). Most of the sediment was emplaced in a series of large submarine fans, which in places are hydrocarbon-bearing today. These fans are well imaged in the areas where they are not masked by basalt flows. It is likely that similar fans extend beneath the basalt flows beneath the Faeroe Shelf.

Conventional seismic profiles

Conventional seismic reflection profiles over the Faeroe shelf with streamer lengths of 6000 m or shorter produce excellent images of the shallow sedimentary section and of the top of the basalt flows, because there is usually a strong impedance contrast between the basalts and the overlying poorly consolidated Tertiary sediments. In Fig. 2 we show examples of the migrated seismic data from lines 1 and 2, using just the 6000 m-long streamer on the lead ship. Later in this paper we show the greatly improved imaging that can be achieved by adding wide-angle data from much larger offsets. Although the shallow sediment section and the top of the basalt flows are imaged well, there is little reliable data from beneath the basalt flows. Such coherent returns as are present beneath the top basalt reflection cannot easily be distinguished from interbed multiples. The highly reflective top of the basalts scatters much of the seismic energy. Short-period ringing, simple and peg-leg multiples obscure weak subbasalt reflections with similar move-out; the high-velocity basalt flows preferentially absorb the higher frequencies in the incident wavelet, degrading the achievable resolution of any subbasalt arrivals; and strong ray-bending caused by large seismic velocity variations between the basalt and sediment may distort the seismic image.

Although little structure is visible below the top basalt reflector in our examples shown in Fig. 2, it is often possible on conventional profiles to see the dominant structure of the flows within the upper part of the basalt section (e.g. Andersen 1988). However, imaging subbasalt structure remains a problem for the reasons mentioned above.

Long-offset seismic profiles

Many of the difficulties facing conventional seismic profiles can be ameliorated by recording data to longer offsets. Most of the multiples produced between the sea-surface, the sea-bed and the top of the basalt layer that contaminate the near-offset wavefield are not present in the wide-angle data because their low apparent moveout velocities mean that they arrive considerably later. Indeed, the first arriving energy at offsets beyond the water-wave cone is always a primary arrival and cannot be a multiple of any kind: this is a considerable asset in imaging because it means that we can interpret the arrivals from such offsets with confidence.

Another advantage of using seismic data from large offsets is that the amplitudes of wide-angle reflections increase toward the critical distance, so at large offsets (large angles of incidence) the reflections often have much larger amplitudes than at short offsets (small angles of incidence). Furthermore, if they are first arrivals at large offsets, the absence of earlier signal-generated noise means that the signal-to-noise ratio of wide-angle reflections is much better than that of near-offset reflections from the same interface, which arrive after other shallower reflections. The seismic velocity control that can be obtained from large-offset arrivals is much better than that deduced from conventional short-offset hyperbolic move-out, thus permitting improved pre-stack depth migration and imaging of deep basement arrivals and enhancing the geological constraints that can be placed on the crustal layers. Finally, there is a greater possibility of recording converted shear waves at wide angles, and these may be useful for both imaging and for constraining the rock types and properties. We show examples of all of these improvements in this paper.

The lengths of hydrophone streamers, and therefore the maximum offsets achievable using a single streamer, have increased steadily over the past three decades. In the 1970s, 2400 m was a normal streamer length, but this has increased as the benefits of recording to increased offsets have become apparent and as digital technology has been incorporated within streamers. 'Normal' streamer lengths for offshore surveys have increased from 2400 through 4000 to 6000 m, until by the year 2000, 12 000 m streamers were deployed for specialist surveys. If even greater offsets are required they can be achieved by building synthetic aperture profiles using two seismic acquisition vessels (Stoffa & Buhl 1979). The maximum offset achievable is limited only by the number of passes that are made by the two ships at different separations (White *et al.* 1999).

The long-offset data used in this paper were acquired for the FLARE project using three passes of two ships to reach offsets of 38 000 m for profiles 1 and 2 (Fig. 1), and a single pass of two ships, each towing 6000 m streamers, to reach offsets of 18 000 m for profiles 4–9 (Fig. 1). Profiles 1 and 2 were acquired in 1996 by Western Geophysical and the Amerada Hess Limited Faeroes Partnership (LASMO (ULX) Limited, Norsk Hydro a.s. and DOPAS) (see White *et al.* 1999 for acquisition details), and profiles 4–9 were acquired in 1998 by Schlumberger Geco-Prakla for the same partnership. Before processing, the data recorded by alternate flip-flop

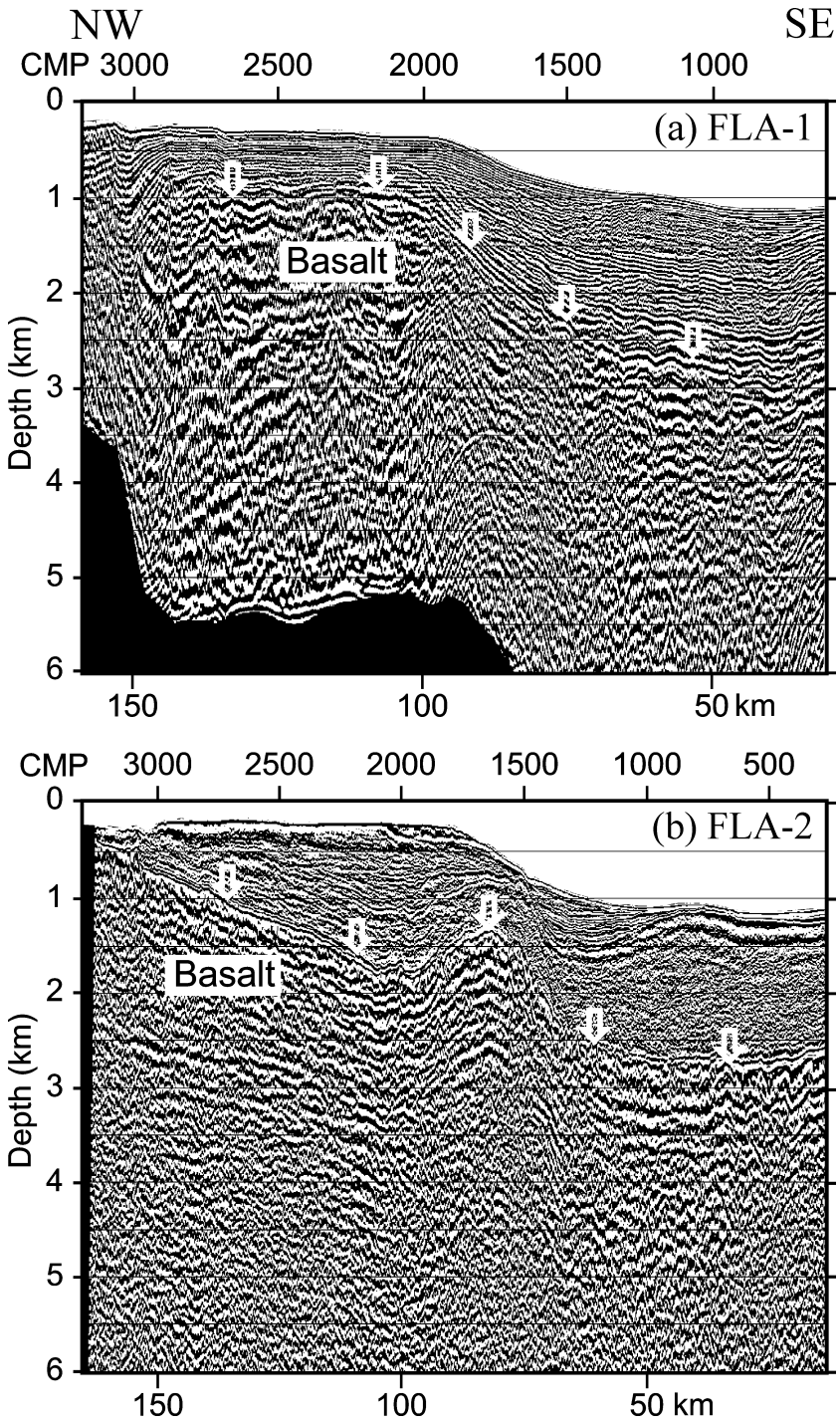

Figure 2. Depth-migrated images of conventional 6000 m streamer profiles along (a) FLARE line 1 and (b) FLARE line 2 (see Fig. 1 for location). The top of the basalt flows (marked by arrows) and the overlying Tertiary sediments are imaged well, but there is little reliable data visible beneath the basalts.

firing of the seismic sources on the two ships was resorted and binned into 'supergathers' (e.g. Fig. 3a) to mimic the data that would have been recorded by a single shot into the synthesized array (for details see White *et al.* 1999). This process assumes reciprocity of traveltimes between the source and the receiver and, more importantly, assumes local 2-D structure (i.e. that the structure does not vary significantly in a cross-line direction within the bounds of streamer feathering).

VELOCITY MODELS FROM WIDE-ANGLE TRAVELTIMES

The variations of traveltime with offset of both reflections and diving waves picked manually from a subset of the shot supergathers were used to create 2-D velocity models along each of the seismic profiles (Fig. 4). These velocity models clearly delineate the extent and thickness of basalt flows on the Faeroes Shelf, together with

lower-velocity sediments that lie beneath them and, in some places, strong reflections off the top of the underlying basement.

We use picks of the main horizons (seafloor, up to three sedimentary horizons and the reflection off the top of the basalt) from the stacked time section as a starting model to ray trace and invert the main wide-angle arrivals from the supergathers. This enables us to construct velocity models of both the shallow section and of the deeper layers. Phases were picked on a subset of the available supergathers using every tenth gather, thus producing one source per kilometre. The ray tracing program 'rayinvr' (Zelt & Smith 1992) was used to invert the traveltimes and thus to build the velocity models.

The velocities in the shallow sediments are constrained well by the moveout of wide-angle reflections: they are mainly terrigenous Tertiary sediments with velocities mostly lower than 3000 m s^{-1}. There is an abrupt increase in seismic velocity at the top of the basalt flows with basalt velocities being well constrained by the first arrival diving waves (red rays in Fig. 3). Reflections off the top of the deeper basement (blue rays, Fig. 3), and diving waves through the basement (cyan rays, Fig. 3) produce strong seismic arrivals at offsets usually in excess of 10 000 m (Fig. 3a): this highlights the usefulness of long-offset data, since these phases are only produced as first arrivals at large offsets. The amplitude of reflections increases toward the critical distance, so the wide-angle reflections here have large amplitudes at bigger offsets. It is these wide-angle arrivals that enable us to build a good velocity model of the deep structure.

The presence of low-velocity sediments beneath the basalt flows is indicated by the step-back of first arrivals at large offsets. In the example supergather shown in Fig. 3(a), the basalt thickness is 1.5 km, and the basalt diving ray terminates at approximately 12 000 m offset because the velocity gradient in the basalt layer is such that raypaths cannot penetrate deeper into the basalt without going through its base (Fig. 3b). The range at which the basalt diving wave terminates depends primarily on the basalt thickness and its vertical velocity gradient (Fliedner & White 2001b). In reality, because the energy travels as waves, the amplitude of the basalt diving wave does not drop abruptly to zero at the far offsets, but decreases more gradually until it is beneath the background noise level. It is also possible for there to be low-velocity sediments beneath a high-velocity basalt layer without a step-back in the traveltimes of the first arrivals appearing on the wide-angle gathers, depending on the combination of velocities, velocity gradients, basalt thickness, local structure and maximum offset recorded.

The velocity in the sediments beneath the basalts is difficult to determine directly. The amplitude versus offset behaviour of the base-basalt reflection may assist in constraining the underlying velocity (Fliedner & White 2001b), and if the base of the basalt can be defined clearly and there is also a strong underlying basement reflection, then the moveout of the basement reflection may help in constraining the intervening sediment velocities. However, often other information has to be used, such as measurements from regional boreholes through the same interval of sediments (Knox *et al.* 1997; Ogilvie *et al.* 2001), or extrapolation laterally from regions further east beyond the feather edge of the basalt flows where conventional moveout measurements can be used to measure the seismic velocity in the same interval of sediment.

These approaches indicate a fairly narrow range of velocities between 3500 and 4500 m s^{-1} for the subbasalt sediment in the area of our survey on the Faeroes shelf. This is considerably higher than the average velocity in the younger sediments above the basalt flows, but still lower than the average basalt velocity of 5000 m s^{-1}, causing the step-back in the wide-angle first arrival, which can be observed in most of our supergathers, and which is diagnostic of a subbasalt low-velocity zone.

The velocity models along each seismic profile derived from matching the traveltimes from ray tracing are shown separately in Fig. 4, and as a fence diagram in perspective view in Fig. 5. They show the main features of the sediment and basalt distribution, and are used as the starting model for the subsequent migrations of the wide-angle seismic data. Although the resolution of these models is relatively coarse, they are sufficient to show the top and the base of the basalt flows, with the total basalt thickness varying between zero in the southeast to more than 3000 m in the west. The basalts subcrop beneath the seafloor near the Faeroe Islands and the top of the basalts increases in depth to more than 2000 m below the seafloor toward the southeast. The thickness of the underlying sediments above the high-velocity layer that we have called the seismic 'basement' in previous publications (Fliedner & White 2001b; Fruehn *et al.* 2001) reaches more than 2000 m.

PRE-STACK DEPTH MIGRATION IMAGING OF WIDE-ANGLE ARRIVALS

After the 2-D velocity model of each line has been derived from the traveltimes of the main arrivals, the raw seismic data can be migrated to produce an image of the subsurface. This has the potential to image details of the structure that are poorly resolved in the velocity models, which used only one set of traveltime picks from every tenth shot gather, and to show details of the structure between the main horizons from which traveltimes were picked.

In principle, if the velocity model was sufficiently good, if there was no offline (i.e. 3-D) velocity or structural heterogeneity, and if proper account was taken in the migration process of the marked phase and amplitude variations that occur as energy is refracted and reflected over different distances and at different angles, then it would be possible to migrate all the energy back to the interfaces from which it was reflected, and thus to achieve a good representation of the depths and shapes of the subsurface interfaces. However, not only are most of the caveats mentioned above not satisfied, or only partially satisfied, but the complete seismic data set is also plagued by energy from scattering, from interbed multiples, and by mode conversion from *P* to *S* waves and vice versa. All of these additional arrivals create energy in the image that has not been migrated properly back to its source, and which therefore creates noise on the seismic section. More problematic, because it can lead to misinterpretations, is the problem that much of the energy may remain coherent after migration, and thus produce apparently real reflections at depths of prime interest, although they are, in fact, artefacts. Interbed multiples and converted *S* waves are a particular problem because they have moveout with apparent velocities that are similar to the real velocities in the seismic section, and so may migrate well at similar depths to real primary arrivals.

One way to reduce some of the problems associated with the mismigration of arrivals, such as those arising from conversions and multiples, is to migrate only that portion of the data set that comes from a chosen reflector. In the following sections we describe the results of migrating the very wide-angle (long-offset) arrivals from the base of the basalt and the immediately underlying region, so as to achieve a good image of the base of the basalt. This technique has been demonstrated by Fliedner & White (2001a): here we apply it to FLARE line 2, which crosses a region of 1000–1500 m thick basalt flows (see Fig. 1 for the location). There is a further advantage to migrating the large-offset data, which is that the arrivals are strong

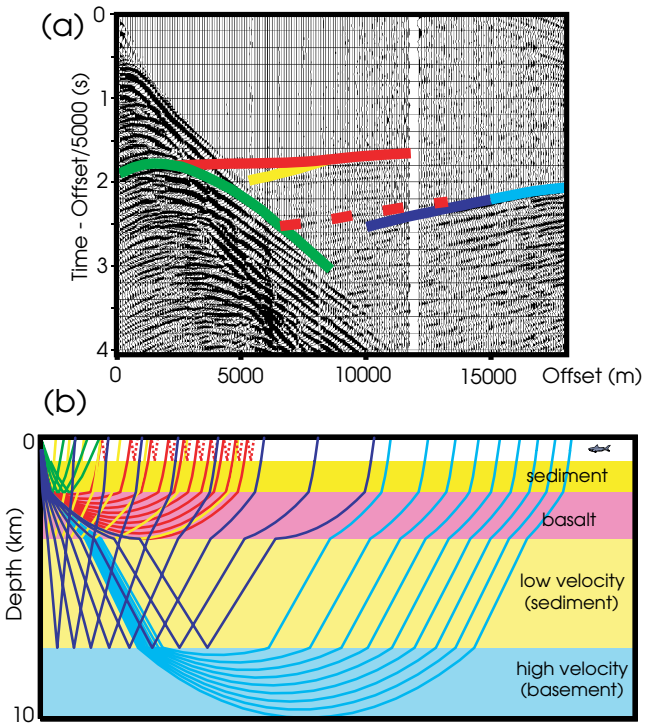

Figure 3. (a) Typical shot gather from line 4 showing main arrival phases in a location where the basalt flows are approximately 2000 m thick. (b) Schematic diagram of raypaths for main arrivals, using the same colour coding as in (a). Green, yellow and blue are reflections off the top of the basalt flows, the base of the basalt flows and the top of the basement, respectively. Red and cyan are diving waves through the basalts and the basement, respectively. Note the step-back of approximately 0.8 s in first arrivals between offsets of 10 000–12 000 m, caused by the low-velocity sediments lying beneath the high-velocity basalt flows.

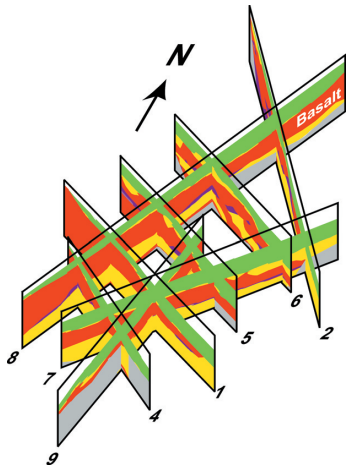

Figure 5. Perspective view of crustal velocity models shown in Fig. 4, viewed from the southeast, using the same colour scheme for velocities as in Fig. 4.

at wide angles, so they produce a high-amplitude image, and they are not polluted by arrivals from the overlying section, as is the case with near-offset data from the same depth. This is because at large offsets, the slower arrivals from the lower-velocity shallower regions arrive much later in the seismic traces. Finally, we have the advantage of being able to migrate both wide-angle *P*-wave arrivals and doubly converted *S*-wave arrivals separately using this technique.

The algorithm employed here is a commercial 2-D Kirchhoff prestack depth migration using maximum-amplitude ray tracing. The events migrated in the wide-angle field are post-critical reflections and the diving wave is a first arrival. Except for the shortest wide-angle offsets, the traveltime difference between the diving wave and the first reflection is negligible; migrating the diving wave thus

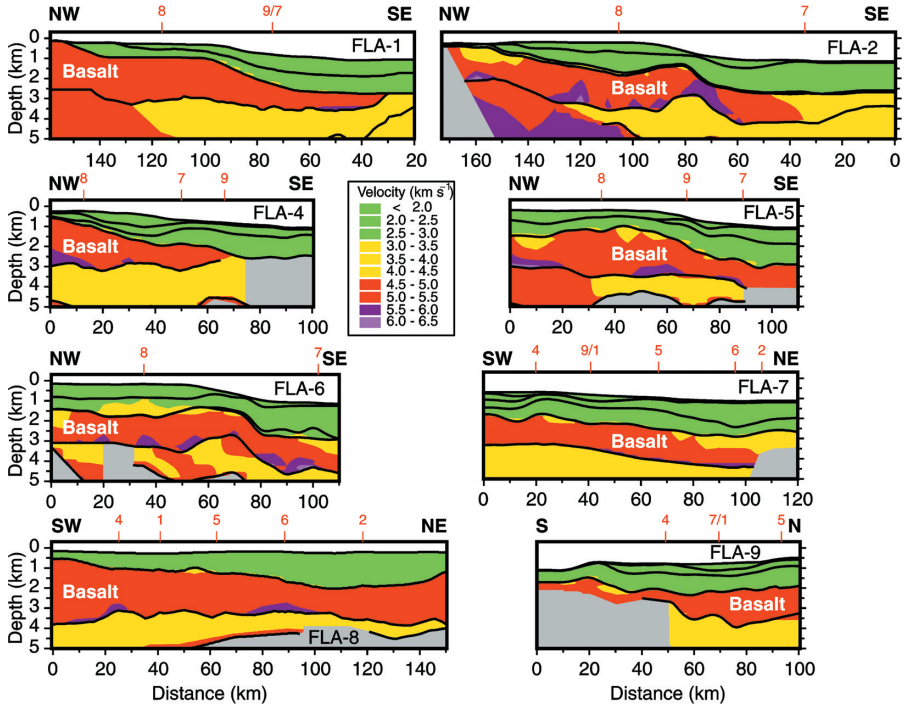

Figure 4. Velocity structure from inversion of wide-angle traveltimes along each of the FLARE profiles shown in Fig. 1. 0 km on the distance scale marks the beginning of each profile as marked in Fig. 1, with shooting in the direction of increasing distance. Red annotations mark intersections between profiles, with solid black lines marking major reflecting interfaces in the velocity models.

introduces some precursor noise in the form of a stretched wavelet that can easily be muted before or after the stack. Amplitudes and phases of the wide-angle image will not be directly comparable with a near-vertical image, but the largest difference will be the frequency content: owing to the preferential absorption of high frequencies along the longer raypaths and the convergence of arrivals in time with offset, wide-angle images lack the resolving power of conventional reflection seismic imaging.

P-wave base-of-basalt and subbasalt reflections

Pre-stack depth migration of the portion of the wide-angle wavefield containing the *P*-wave basalt arrivals, using the 2-D velocity model derived by ray tracing, yields for line 2 the image of the base-basalt and immediately underlying region shown in Fig. 6. This migrated image contains no contribution from the top of the basalt flows or from the overlying sedimentary layers, because they are not present in the part of the wide-angle seismic wavefield that has been migrated.

The shallow sedimentary section and the top of the basalt is imaged best using conventional near-offset data. Therefore, to obtain a depth section that extends all the way down to the base of the basalts from the seabed, we merge the migrated wide-angle image of the base-basalt and underlying sediments shown in Fig. 6 with the conventional pre-stack depth-migrated image of the shallow sediments and the top of the basalt from the near-offset wavefield, to give the composite image shown in Fig. 7. This combines the best features of the conventional near-offset data, including good resolution in the shallow sedimentary section, with the lower-resolution, but high-amplitude wide-angle image of the base-basalt and immediately underlying region. It is particularly easy to see the basalt layer, and its variation in thickness along the profile. Note that on the image shown in Fig. 7, the amplitudes of the base-basalt reflection are not directly comparable with those of the shallower section, because we have taken advantage of the high amplitudes of the wide-angle reflections to produce a strong base-basalt image.

Although the migrated wide-angle reflections are of great value in showing which arrivals are from the base of the basalt, and from deeper in the section, their low-frequency content and the large angles at which reflections occur (and therefore the large size of the Fresnel zone), means that they have a much lower resolution than reflections from closer to normal incidence. So for interpretation purposes it is best to combine a migrated image of the entire data set from normal incidence out to wide angle with the composite image that contains the separately identified and migrated high-amplitude deep arrivals. In Fig. 8 we show an example of this from the central portion of FLARE line 2.

The lower panel of Fig. 8 shows the composite image with the separately migrated base-basalt reflection, enlarged from the profile shown in Fig. 7. The upper panel of Fig. 8 is the pre-stack depth

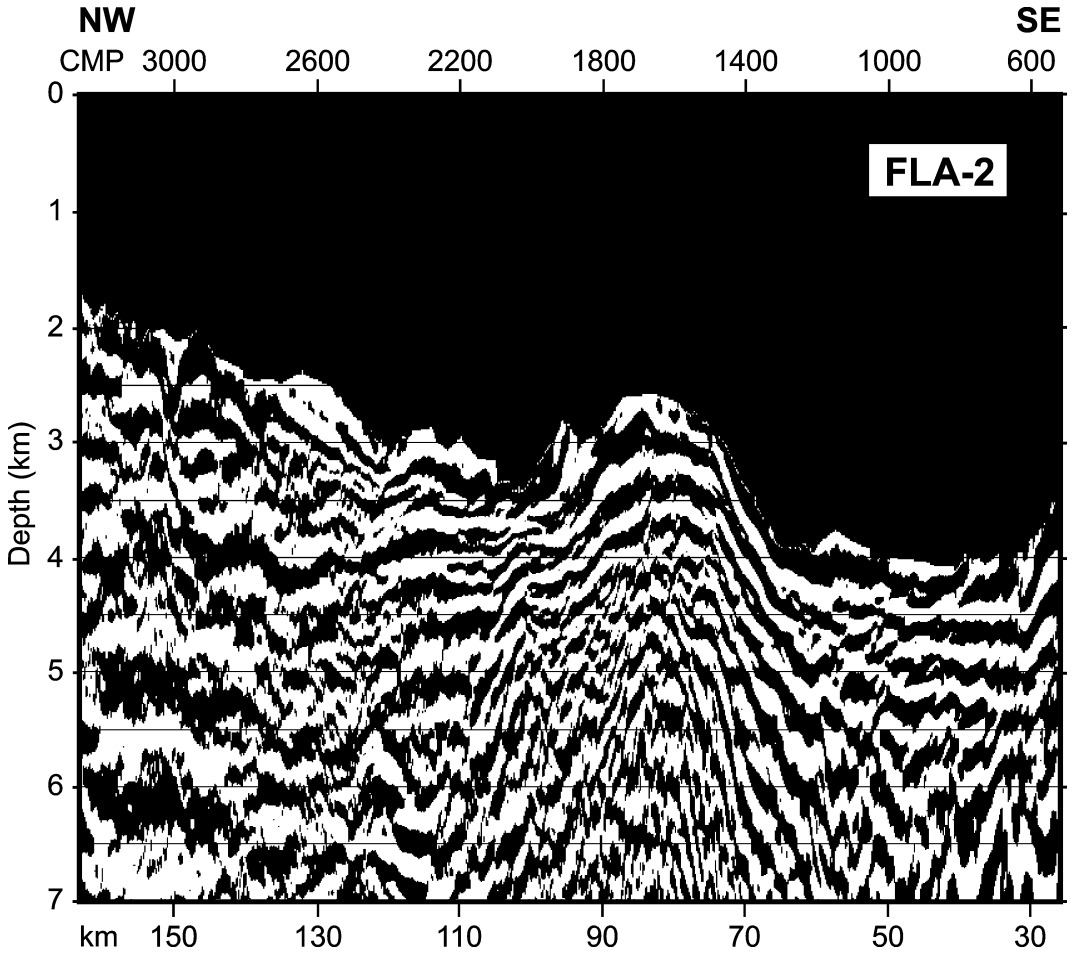

Figure 6. Pre-stack maximum-amplitude Kirchhoff depth migration of the portion of the *P*-wave wide-angle seismic data from line 2 containing the base-basalt reflection using the 2-D velocity model developed from inversion of the traveltimes. Only data outside the cone formed by the direct water wave and the asymptotes of sedimentary and top-basalt reflections have been migrated (see Fliedner & White 2001a).

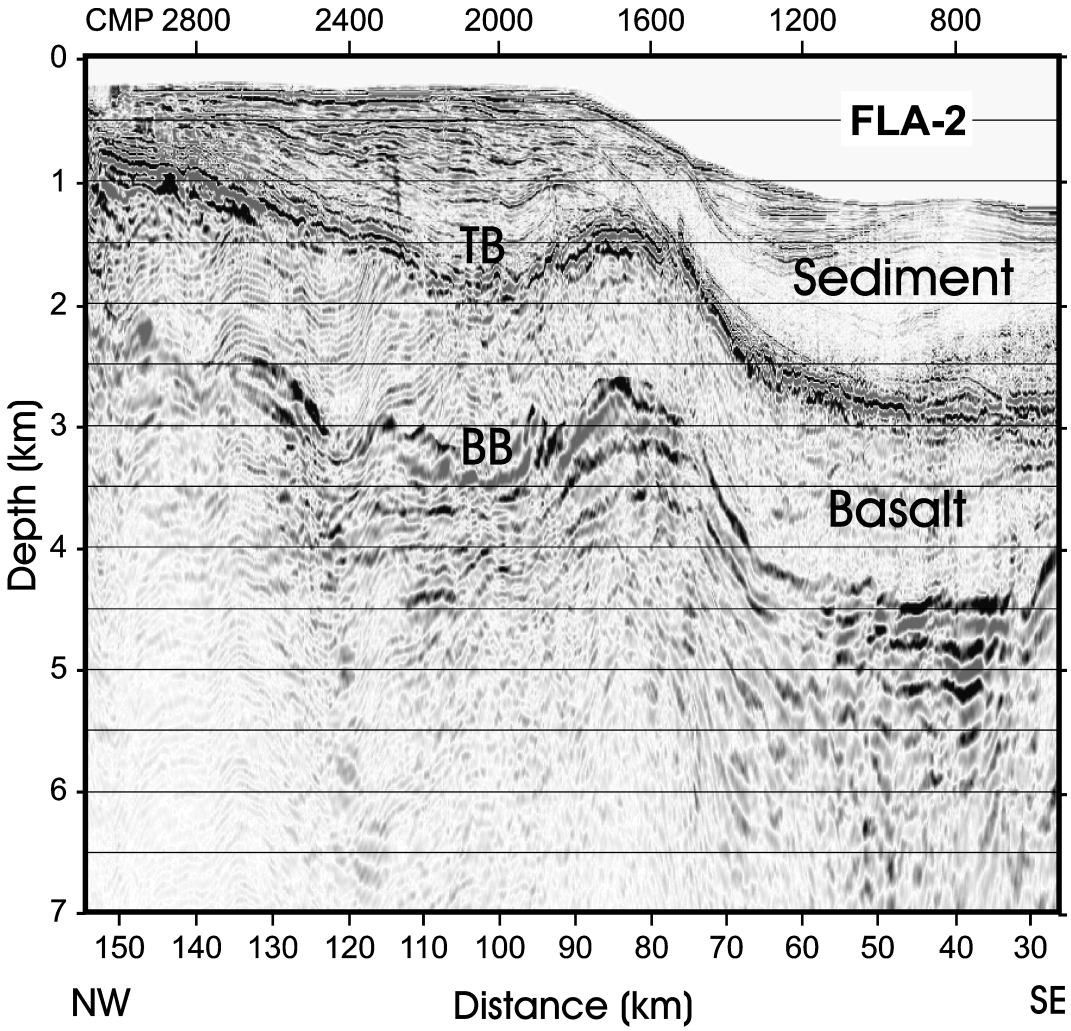

Figure 7. Merged seismic profile along line 2 compiled from migrated image of sediment and top-basalt reflections with the wide-angle migrated image of the subbasalt region superimposed (from Fig. 6). Note that the amplitudes of the top-basalt (TB) and base-basalt (BB) reflections are not directly comparable, since they are normalized independently.

migration of the entire data set for the identical portion of line 2. This uses the best velocity model for the migration derived by utilizing all the wide-angle arrivals. The resolution of the base-basalt arrival in the upper panel is better than that of the lower panel. However, since the upper panel also contains many multiples, it is difficult to know which arrivals are from the base of the basalt and which are artefacts from multiples. Combination of the base-basalt interface identified by wide-angle ray tracing in the lower panel with the pre-stack depth migration in the upper panel allows us to have more confidence in our interpretation of the structure.

Converted *S*-wave base-of-basalt and subbasalt reflections

Marine seismic acquisition using towed near-surface hydrophone streamers allows only the generation and recording of *P* waves, because both the source and the receivers are in the water and fluids do not transmit *S* waves. It is therefore not well suited for *S*-wave exploration. Conventional *S*-wave exploration relies on single mode conversions at the reflector (thus producing *PS* arrivals), and the use of seafloor three-component seismometers to record the converted *S* waves. Lacking ocean-bottom recordings in the FLARE data set, this potentially promising route of subbasalt exploration (e.g. Cowley *et al.* 1999) is not open to us. We investigate instead the potential of using doubly converted waves: these are waves that have been converted from *P* to *S* at some interface, and then have travelled as *S* waves in the subsurface, before being converted back to *P* waves prior to entering the water column on the return path to the surface (these are often termed *PSSP* arrivals).

Among the large number of possible double conversions, we concentrate on arrivals where *P*-to-*S* and *S*-to-*P* conversion takes place at the same interface, because such symmetric arrivals can be processed in the same way as pure *P*-wave arrivals (*PP* reflections), in the common mid-point (CMP) domain. All that is necessary in the processing is that *S*-wave velocities replace *P*-wave velocities in the layers where the converted wave travels in the shear mode. The interfaces that are primarily of interest for mode conversion are the seabed (water/sediment) and the top-basalt (sediment/basalt) horizons because there is good coupling at these interfaces between different modes.

Good mode conversion occurs where the *P*-wave velocity on one side of a first-order interface is similar to the *S*-wave velocity on the other side of the interface (White & Stephen 1980). The *S*-wave velocity of approximately 2700 m s^{-1} expected in the Faeroe basalt

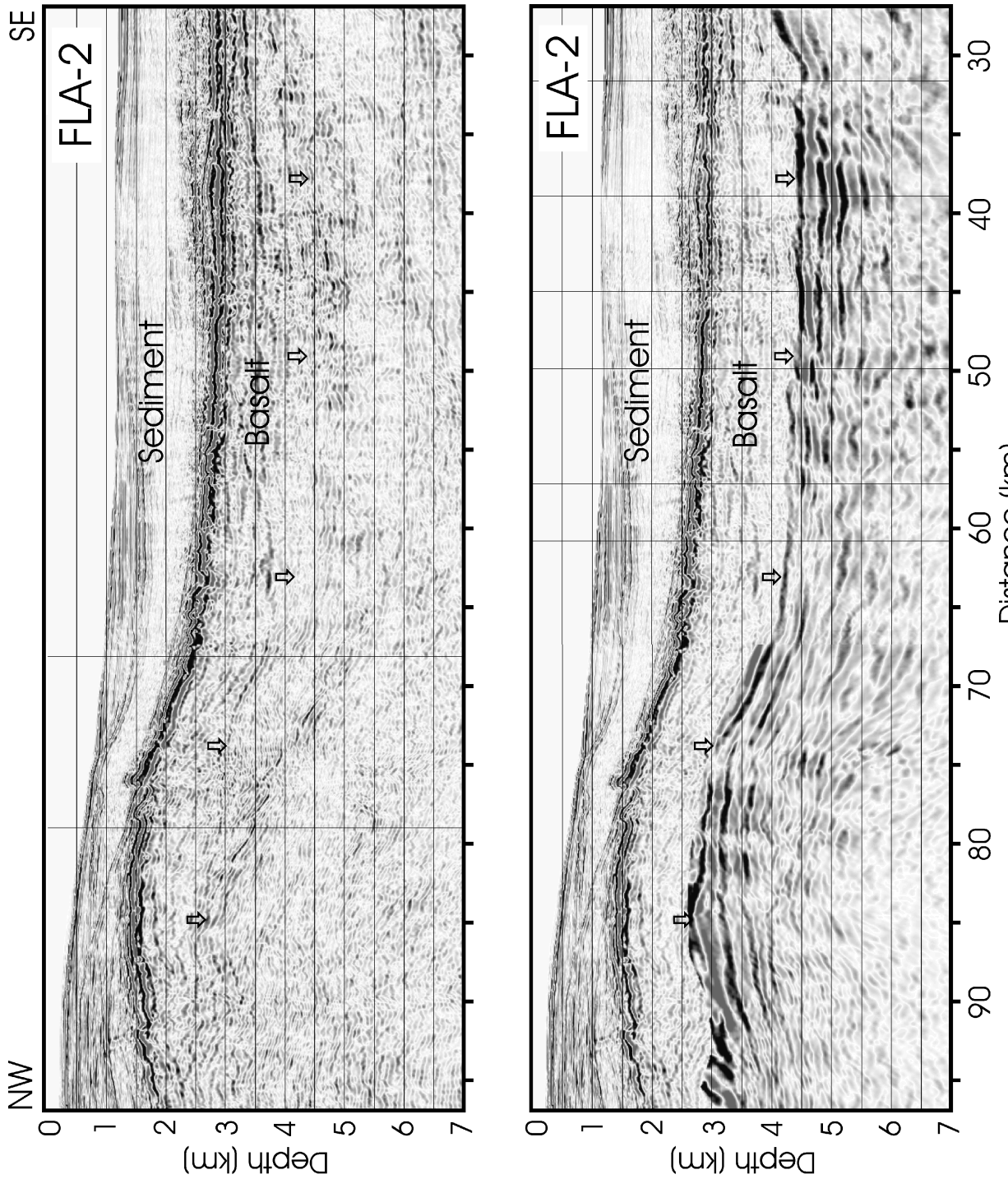

Figure 8. Enlargement of the central portion of line 2 showing (top panel) pre-stack depth migration of the entire seismic data set, and (lower panel) composite image produced by combination of the shallow sediment and top-basalt section with the migrated wide-angle base-basalt arrival (enlarged from Fig. 7). Note the better resolution of the upper panel, but the usefulness for identifying the base-basalt reflector (marked by arrows on both panels), of the wide-angle data in the lower panel.

(*P*-velocity 5000 m s^{-1}, V_p/V_s 1.85; Nielsen *et al.* 1984) is a good match for the sedimentary *P*-wave velocities found directly above the basalt flows in at least some areas of the Faeroe–Shetland Basin. In these circumstances, the top-basalt horizon is a good converter of seismic energy, whether the wave is travelling from the sediment to the basalt or vice versa. The condition of matching sedimentary *P*-wave and basalt *S*-wave velocities is fulfilled, especially along line 2, where a thin layer of consolidated Palaeogene sediments or tuffs (*P*-velocity approximately 3000 m s^{-1}) covers, and removes some of the irregularities in the rugged basalt flow surface; here we observe good converted arrivals from the basalt flows and below.

Inspection of the FLARE supergathers shows that double conversions at the top-basalt interface can be identified in several areas. The best and most continuous converted arrivals appear in the northwestern portion of line 2 (Fig. 9). The example shot gather shown in

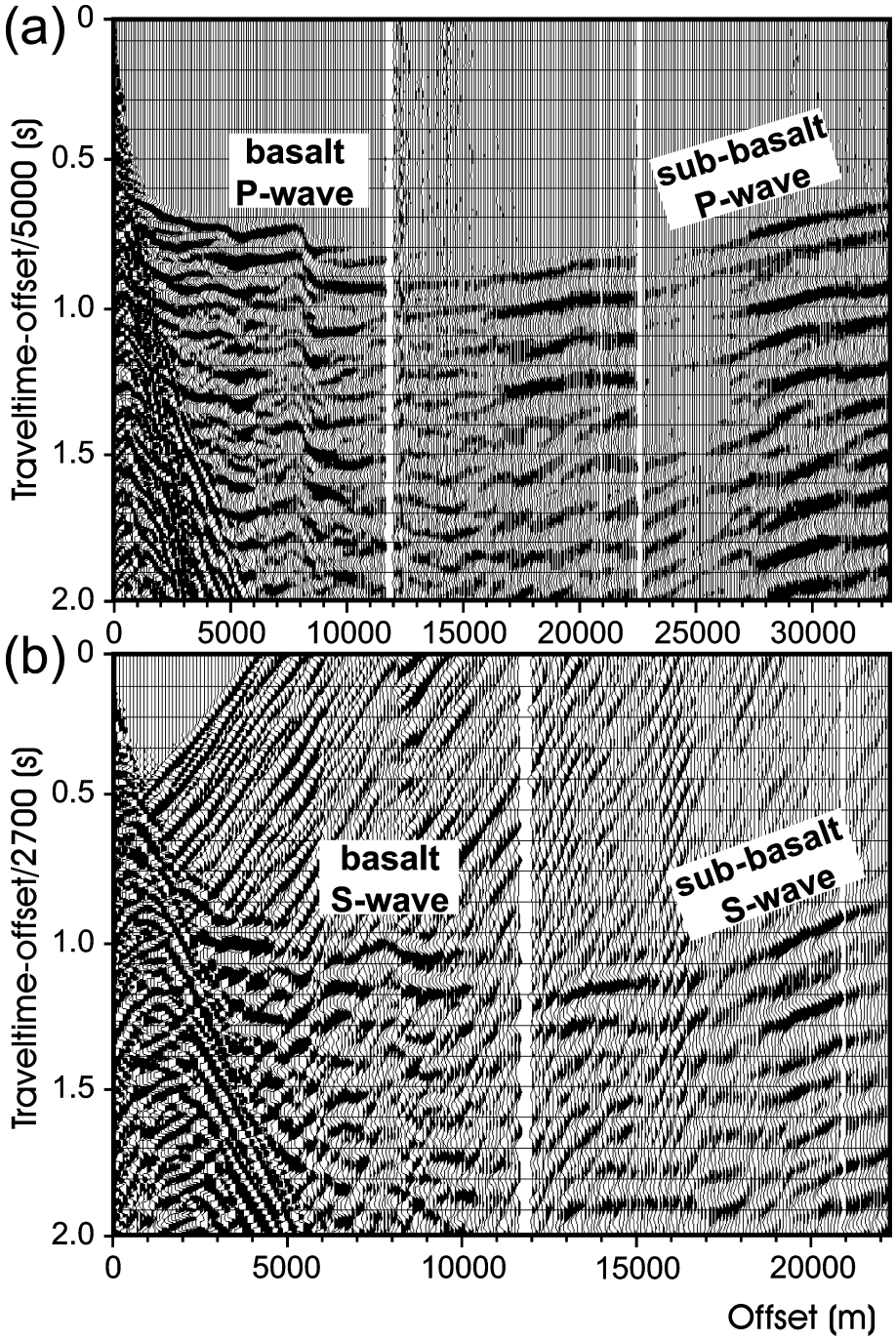

Figure 9. Example of a single shot supergather from line 2, with the shot-point at 160 km along the profile: offsets increase southeastward, and the offset range of 33 000 m spans the interval from 127 to 160 km along the profile (Figs 4 and 7). The 2-D structure along the profile causes irregularities in the arrivals; the data gaps at ∼12 000 m and ∼23 000 m are a consequence of the construction of supergathers using two ships with flip-flop shooting (see White *et al.* 1999 for details). (a) Shot gathers reduced at 5000 m s^{-1} to highlight the *P*-wave arrivals from the basalt and subbasalt layers; (b) the same shot gather reduced at 2700 m s^{-1} to highlight the doubly converted *S*-wave arrivals from the same layers.

Fig. 9 from 160 km on-line 2 (i.e. extending from 127 to 160 km), shows a strong mode-converted wide-angle arrival that mimics the first arrival (*P*-wave diving wave and reflections from the basalt flows, Fig. 9a), but at shear velocity and traveltimes (Fig. 9b). Shot gathers such as this allow good estimates to be made of the average shear wave velocity of the basalt flows in this area, which is within the range of V_p/V_s measurements in the Lopra borehole (Nielsen *et al.* 1984; Kiørboe & Petersen 1995). The Lopra borehole on the southern Faeroe Island of Suduroy (Fig. 1), penetrates a thick section of the Lower Series Basalt flows, which can be traced across the adjacent Faeroe Shelf (Ritchie *et al.* 1999), and so provides useful constraints on the physical properties of these basalts.

In the same manner as used for the *P* waves, here we migrate just the wide-angle part of the mode-converted seismic wavefield. Note, however, that a converted arrival emerges at a shorter offset than the equivalent pure *P*-wave arrival through the same layers, because the *S* wave has a lower velocity and therefore a steeper raypath than does the *P* wave. By using a single V_p/V_s value of 1.85 for the basalt layer, we have produced a depth image of the base-basalt reflection with waves doubly converted at the top-basalt interface. This can be compared directly with the pure *P*-wave image obtained earlier (Fig. 7). As before, we have made a composite image by adding the wide-angle migrated image of the base-basalt region to the conventional pre-stack depth migration of the shallower section. The *PP* image (Fig. 10a) and the *PSSP* image (Fig. 10b) of the base-basalt reflection are similar in depth and shape, giving confidence that we have imaged a doubly converted *S* wave, which underwent double mode conversion at the top basalt interface, and which travelled through the basalt as an *S* wave.

It is clear from Fig. 10(b) that there are coherent arrivals across tens of kilometres on the *PSSP* profile. The precise shape of the reflections is not, however, identical on the *PP* and the *PSSP* images, although there are broad similarities. Assuming that we have correctly identified these arrivals as doubly converted *S* waves, there are several factors that could cause differences between the *PP* and the *PSSP* images. The most likely reason is that mode conversion occurred at slightly different horizons along the profile. Another likelihood is that the ratio of *P*- to *S*-wave velocity varies along the path of the converted *S* wave within the basalt section: the layered, cracked nature of the basalt, together with the possible presence of interbed sediments, of weathered horizons and of tuffs or rubble, make this highly probable. Furthermore, of course, any errors in our estimation of the *P*-wave velocity would cause misfits in depth when the *PP* and *PSSP* images are compared, even if we used exactly the right ratio of *P*- to *S*-wave velocity.

A final reason for differences between the *PP* and *PSSP* images could be that since the *P* and *S* waves have wavelengths that differ by almost a factor of 2, they will 'see' gradational interfaces differently, since the reflectivity of a reflector depends on how sharp it is compared with the wavelength of the incident seismic energy (e.g. White & Stephen 1980). The base of the basalt flows is probably a complex mixture of baked sediments, tuffs, ashfall and lava flows, which produces a gradational velocity change from the interior of the basalt flows to the underlying sediments. So we might expect *P* and *S* waves to 'see' different reflecting interfaces from a complex base of the lava flows.

Though the *PSSP* image in Fig. 10(b) is only a first attempt at imaging using mode-converted shear waves, the coherence of the reflections provides encouragement that this technique may yield fruitful results in the future.

PRE-STACK DEPTH MIGRATION OF THE ENTIRE SEISMIC WAVEFIELD

Detailed velocity model from iterative depth migration

After obtaining a pre-stack depth-migrated image with the initial velocity model, it is possible to improve the velocity model within and below the basalt flows iteratively by picking migrated horizons and ray tracing their reflections, refractions, multiples and conversions in the shot domain. Horizons down to the top of the basalt can be traced easily after simple time processing and multiple removal (see also Fruehn *et al.* 2001). Deeper horizons only become apparent after ray tracing of the wide-angle arrivals in the supergathers and subsequent depth imaging. In this section we show the results of deeper imaging, down to the basement well below the basalts, using FLARE line 1 as an example.

In Fig. 11(a) we show CMP gathers from three locations along FLARE line 1. Each gather is reduced at a velocity of 5000 m s^{-1} to emphasize the wide-angle arrivals (an arrival with a phase velocity of 5000 m s^{-1} is horizontal on a reduced shot gather). Examples of some of the horizons that we used for the ray tracing velocity modelling are marked in Fig. 11. Where the basalt section is thick, it is often possible to see separate arrivals on the wide-angle gathers from diving waves that are refracted within the basalts (e.g. 'B' on CMP 2500 at 125 km in Fig. 11a), and from energy reflected at wide angles from the base of the basalt (e.g. 'BB' on CMP 2500, Fig. 11a). Careful analysis of the amplitude versus offset behaviour of the wide-angle basalt arrivals adds further constraints to the velocity structure within the basalt section. Detailed internal velocity gradients in the basalt flows along line 1 are discussed further by Fliedner & White (2001b).

CMP-gather 750 (at 37.5 km along profile 1) is located near the eastern feather edge of the basalt flows and shows the short wide-angle basalt arrival produced by a turning wave in the basalt layer (B) just emerging from the strong water wave (WW) cone. The top of the basalt (TB) is a strong reflector, which produces a coherent hyperbolic reflection from normal incidence out to wide angles. Since the thin basalt flows in this area produce only short basalt arrivals, the large-offset wavefield is dominated by arrivals from the deeper sedimentary section and the underlying crystalline basement. These arrivals from deeper in the section can be traced from CMP 750 westward from gather to gather (increasing CMP numbers) beneath the thickening basaltic cover.

The characteristic step-back associated with a thick low-velocity zone underlying the basalt can be seen clearly in these gathers. As the basalt thickens (increasing CMP number, further west along the profile), this step-back moves to increasing offsets until it can no longer be recorded within the supergather spread because it lies beyond the maximum offset of the recorded data. Wide-angle image gathers after depth migration, from the same CMP locations are shown in Fig. 11(b). A combination of the arrivals seen on the CMP gathers with the image gathers allows us to identify arrivals from specific horizons and then to trace them across the seismic profile.

The deepest reflections on the CMP gathers are from the lower crust (LC), and generally produce strong arrivals at large offsets and large two-way traveltimes. They come from depths of 10–12 km below the surface and probably represent Lewisian crust. Between the basalt turning wave (B) and the lower crustal arrivals (LC) are several wide-angle arrivals (e.g. X, Y), from the subbasalt section. These come from depths of 4–7 km, and probably represent

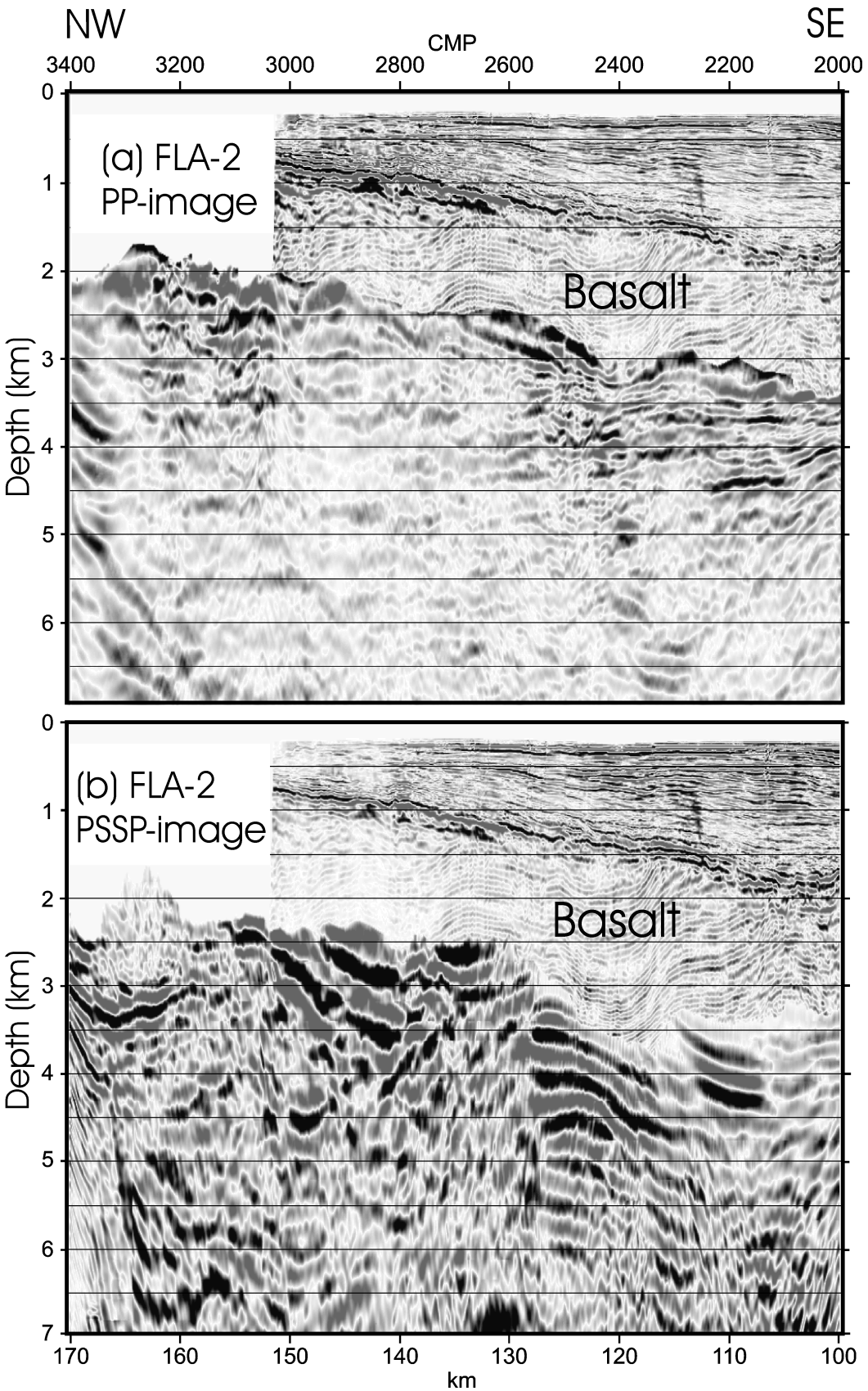

Figure 10. Comparison of base-basalt images derived from (a) pre-stack depth migration of *P*-wave wide-angle arrivals, as in Fig. 7; (b) pre-stack depth migration of wide-angle arrivals doubly converted to and from *S* waves at the top-basalt interface. In both cases the migrated wide-angle base-basalt images are superimposed on the sediment and basalt reflections derived from conventional short-offset *P*-wave migrations. Note the similarity in the depth image between the *P* wave and doubly converted *S*-wave base-basalt images, and the possibility of enhanced structural resolution by also using the converted *S*-wave image.

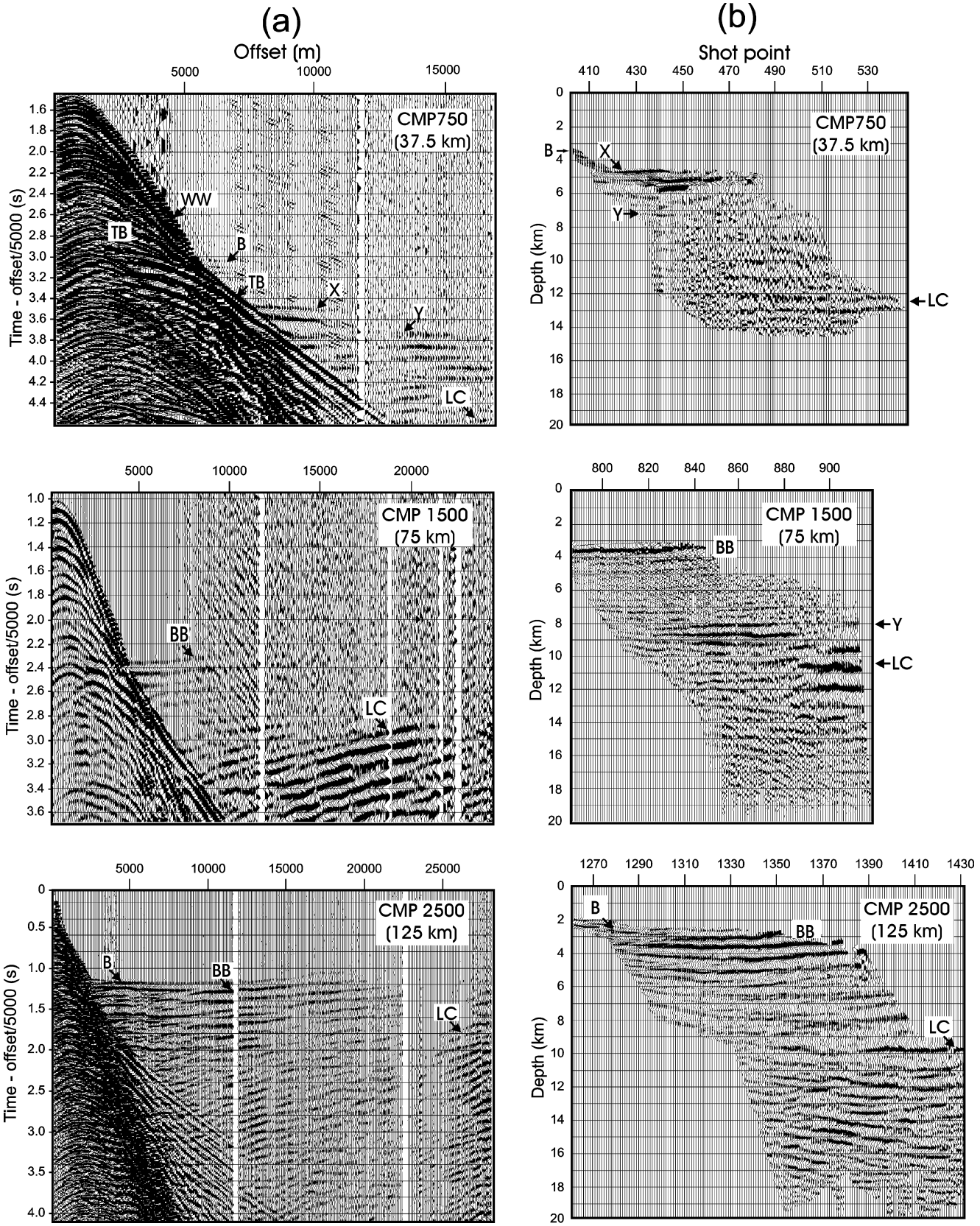

Figure 11. (a) Typical CMP gathers from line 1 from a location where basalt flows are just thick enough to be observable at wide angles (CMP 750, at 37.5 km) to a location where basalt flows are almost too thick to see a subbasalt low-velocity zone (CMP 2500, at 125 km). Note that variable time and offset scales are used to allow different arrivals to be seen clearly. TB marks hyperbolic reflection from the top of the basalt; BB is reflection from the base of the basalt; B is basalt diving wave; X, Y are subbasalt sedimentary arrivals; LC marks reflections that arrive probably from the Lewisian crystalline basement. (b) Depth-migrated wide-angle image gathers at the same CMP locations.

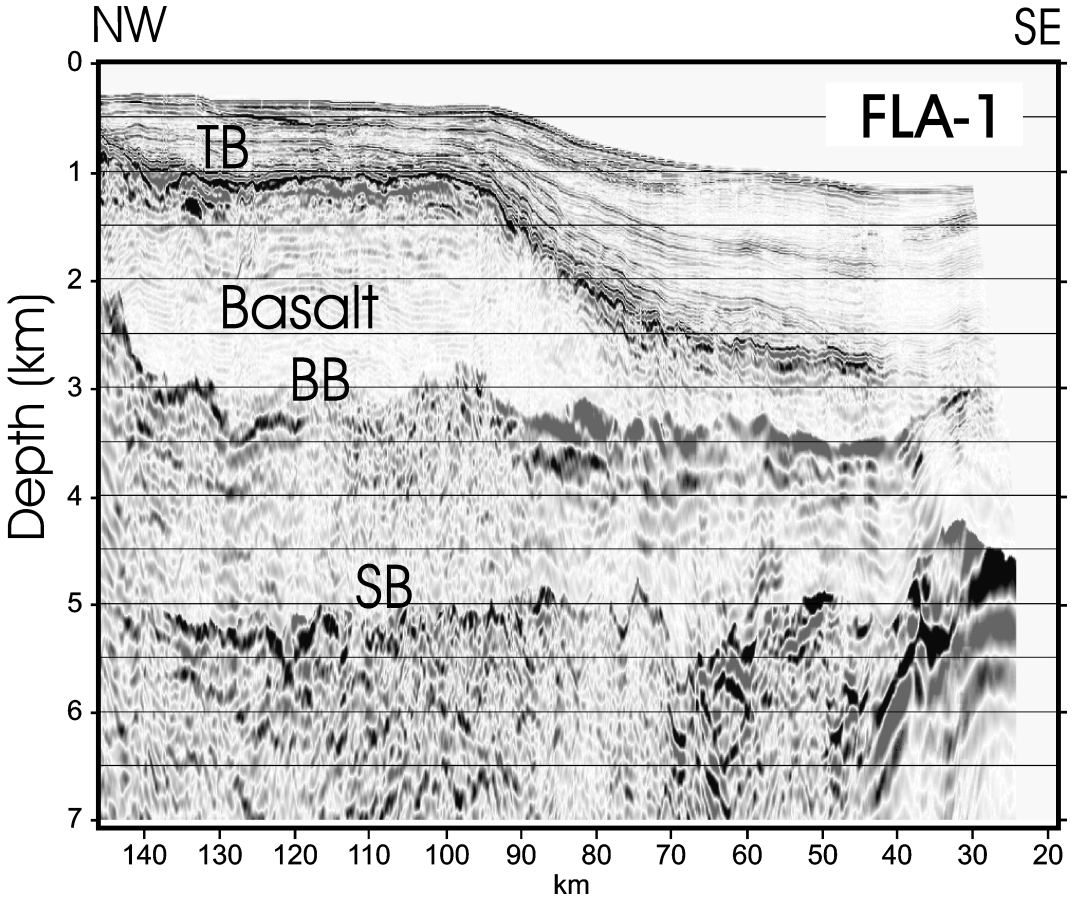

Figure 12. Merged seismic profile along line 1 compiled from migrated image of sediment and top-basalt (TB) reflections with the wide-angle migrated images of the base-basalt (BB) and subbasalt (SB) arrivals. Note that the amplitudes of the top-basalt, base-basalt and subbasalt reflections are not directly comparable, since they are normalized independently.

reflectors from the Mesozoic sedimentary section that was deposited in this region following earlier episodes of rifting.

A composite image of the strongest continuous deep reflectors can be built up using the base-basalt and deeper wide-angle arrivals in the same manner as already described for line 2. The image for line 1 obtained in this way is shown in Fig. 12, where the top-basalt (TB) and base-basalt (BB) arrivals have been migrated separately, as also have arrivals from a deeper, discontinuous subbasalt (SB) horizon some 2000 m beneath the base of the basalt.

P-wave image of the entire seismic wavefield

Once the final velocity model has been built up, pre-stack depth migration of the entire data set from normal incidence to wide-angle produces the image for line 1 shown in Fig. 13. Superimposed in colour are the velocities of the rocks, which together with the identification of prominent horizons made possible by the long-offset data, provides a good depth image of the geological structure.

Within the basalts themselves, the intrabasalt reflectivity may be very complex. The wavelength of the seismic energy is much greater than the thickness of individual flows, so the overall seismic response of the basalt section is produced by interference between energy returned from multiple flows, which themselves often have a complex impedance structure arising from weathered tops and bases (Smallwood *et al.* 1998; Fliedner & White 2001b). The seismic velocity of the flows increases with depth, probably due both to crack closure with depth, and to the larger average flow thickness of the Middle Faeroes basalt flows, which form the lower portion of the submarine basalt section on the Faeroe Shelf compared with the thinner flows of the Upper Faeroes Series, which is found in the uppermost part of the basalt flows: since the weathered tops of individual flows generally have lower seismic velocities than the unweathered, massive interiors, a preponderance of thinner flows means that they contain a greater proportion of lower-velocity weathered basalt and interflow soils, thus lowering the overall average velocity compared with a sequence of thick flows.

Immediately beneath the basalts the seismic *P*-wave velocity decreases by approximately 1000 m s^{-1}. This is shown in Fig. 13 by a change to cooler colours. This velocity decrease is constrained not only by the traveltimes of the wide-angle reflections, but also by detailed analysis of the amplitude-versus-offset behaviour of the waveforms reflected at wide angles from the base of the basalt (see Fliedner & White 2001b for details of the velocities along line 1 constrained by this method).

The low-velocity material beneath the basalts represents sedimentary rocks, though in the absence of any deeply penetrating wells on the Faeroes Shelf, the precise age and rock type of the sediments is at present uncertain. However, to the southeast of the Faeroe Islands, subbasalt reflections can be imaged dipping beneath the feather edge of the basalts from the region of the Faeroe–Shetland Trough where basalts are absent (Fig. 13). By correlation with wells beyond the feather edge of the basalts, it is clear that the Faeroe basalt flows overly early Palaeocene strata (Ebdon *et al.* 1995;

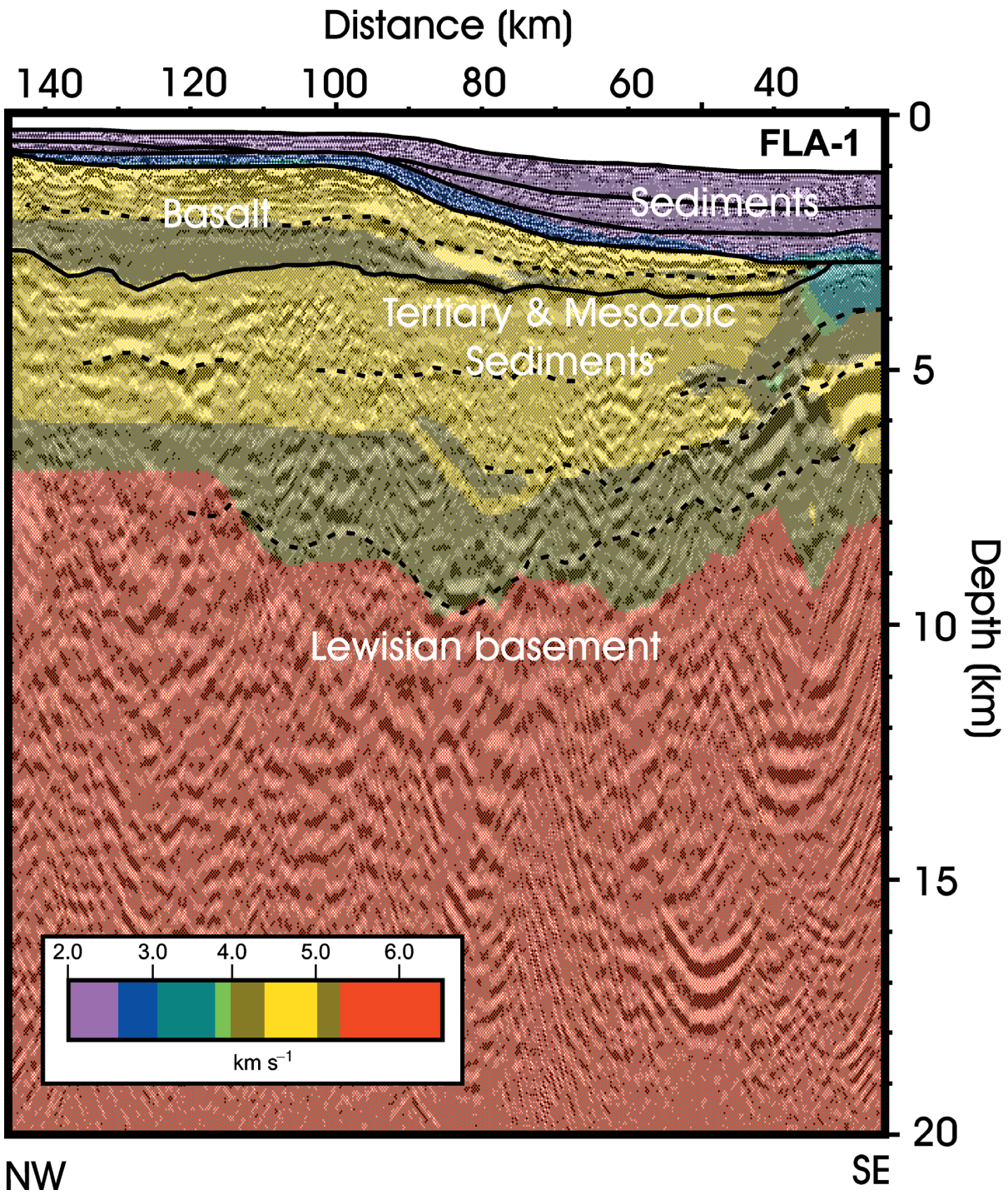

Figure 13. Final velocity model (in colour) for line 1 derived from ray tracing of arrivals picked from every tenth supergather (i.e. every kilometre). This velocity model was then used to produce by pre-stack depth migration of the superimposed seismic image from line 1. Some major interfaces identified by the raytrace modelling are highlighted by solid and broken lines.

Jolley *et al.* 2002). The deeper reflections under the basalts (Fig. 13) are probably caused by Cretaceous and other Mesozoic sections that, in turn, overlie much older Caledonian and Archaean crust. In the adjacent Faeroe–Shetland Trough the pre-Tertiary sediment thickness reaches 8000 m (Stoker *et al.* 1993). Our profiles suggest that this pre-Tertiary sediment section continues beneath the basalts, although it is thinner in the region of our profiles, only reaching 3000–4000 m thickness, and thins towards the Faeroe Islands. Gravity modelling along profiles adjacent to FLARE lines 1 and 2 also suggests subbasalt sediment thicknesses reaching 3000–4000 m in this region (Smallwood *et al.* 2001). There is evidence on our seismic profiles of discontinuous short reflections within this deeper subbasalt section, for which the best interpretation is that they are caused by fault blocks created during rifting episodes that occurred from the Permian to the early Palaeocene.

The velocity model helps distinguish between the lower-velocity subbasalt Mesozoic and Phanerozoic sediments and the higher velocity underlying Archaean Lewisian crust. The Lewisian

metamorphic crust on the northwest British margin has *P*-wave velocities ranging from 6100 to 6200 m s^{-1} in the upper portion, to 6400–6600 m s^{-1} in the deeper section (Hall & Simmons 1979; Jones *et al.* 1984).

Within the crystalline basement there are few coherent reflectors that can be identified unambiguously as primary reflections. An exception is the 10 km long flat-lying reflection at 12 km depth, approximately 30 km along line 1, and another possible reflection of similar lateral extent at 16 km depth, some 50 km along line 1 (Fig. 13). These high-amplitude, coherent reflections may be caused by basaltic sills intruded in the mid-crust. At the northwestern end of line 1, layered reflectivity in the lower crust is seen at the furthest offsets of the supergathers (20–38 km offsets). Similar layered lower crust is observed on many profiles on the northwest British continental margin (Matthews & Cheadle 1986), and may in this case represent lower crustal intrusion of Tertiary igneous sills (Richardson *et al.* 1999).

Very long-range arrivals from the offshore shooting along line 1 recorded by land stations on the Faeroe Islands include wide-angle reflections interpreted as coming from the Moho at the base of the crust. These constrain the total crustal thickness along line 1 as varying from 20 km at the southeast end to 25 km at the northwest end (Richardson *et al.* 1999), crustal thicknesses that are confirmed by gravity modelling (Smallwood *et al.* 2001).

CONCLUSIONS

The combination of conventional hydrophone streamer data from short offsets (0–6000 m) with wide-angle data from very long-offset recordings (up to 38 000 m in the FLARE data used in this paper), allows good imaging of the top and base of the basalt flows, and improved imaging of the subbasalt structure. The fence diagram of composite pre-stack depth migrated data from the top and bottom of the basalts shown in Fig. 14 illustrates the main basalt structure on the Faeroes Shelf, using three representative profiles (FLARE profiles 1, 2 and 7; see Fig. 1 for the location). An unfolded display along portions of these three profiles shown in Fig. 15 illustrates

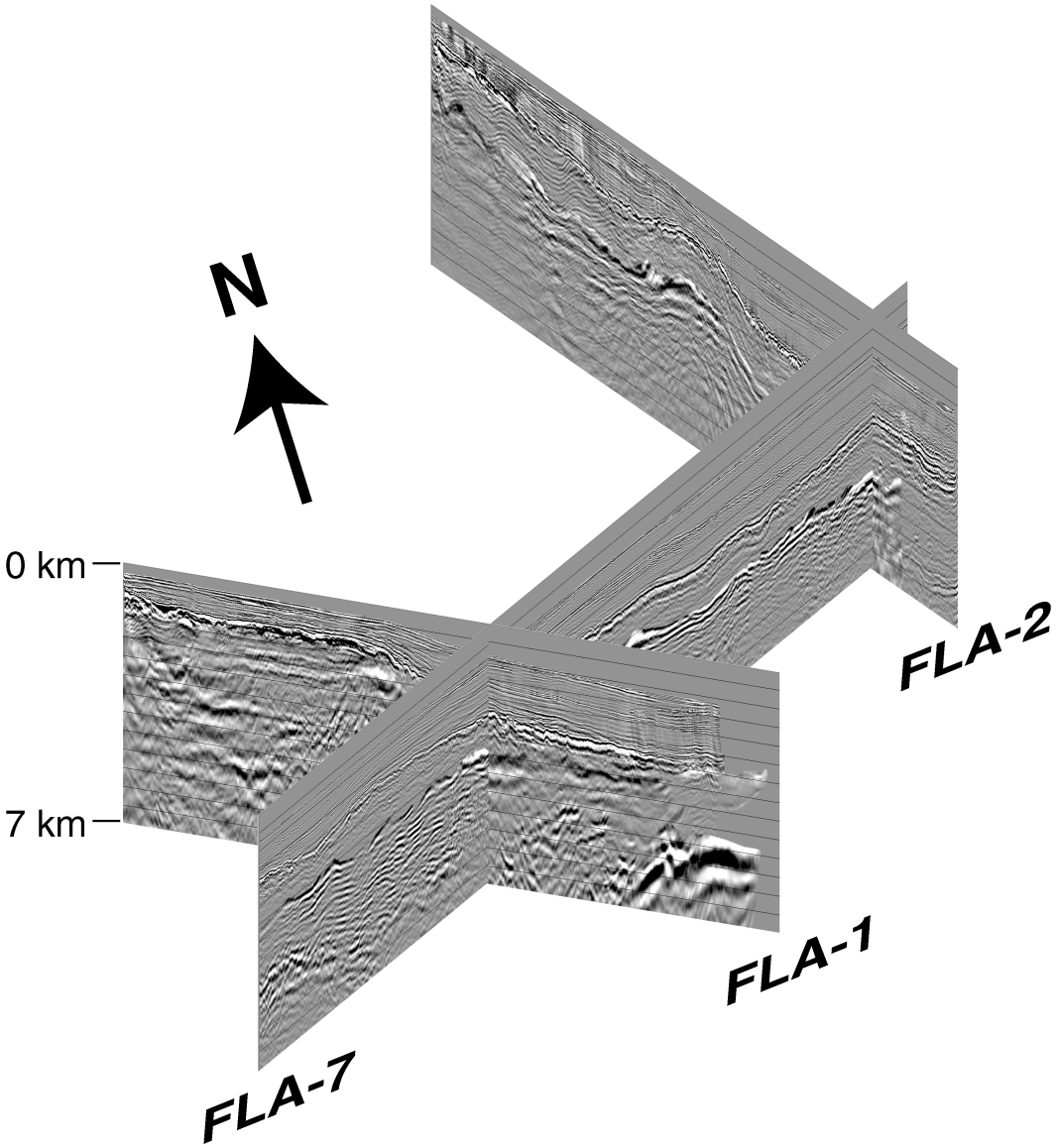

Figure 14. Perspective fence diagram of the seismic sections combining lines 1, 2 (from this study) and 7 (from Fliedner & White 2001a). See Fig. 1 for line locations.

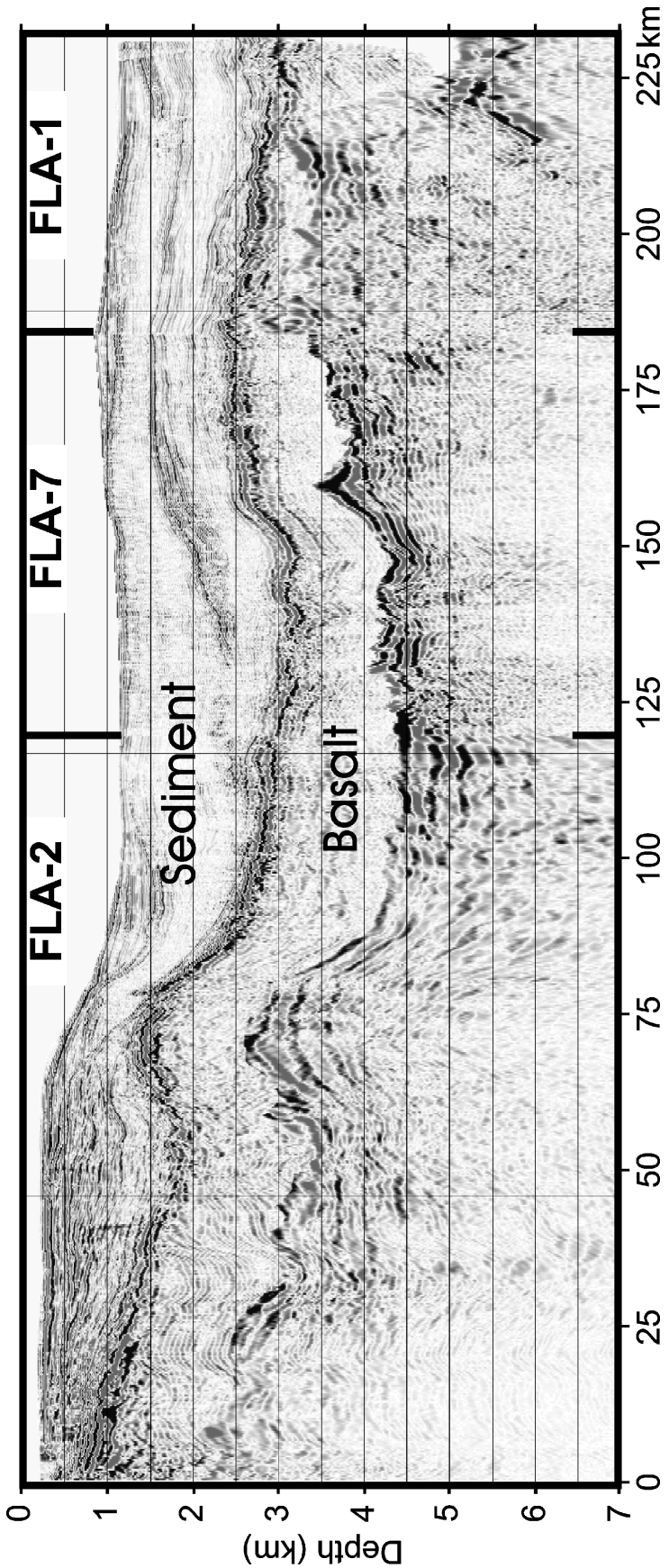

Figure 15. Unfolded seismic section, highlighting the top and base of the basalt flows from lines 1, 2 and 7 (see Fig. 14) along the line marked by solid lines in Fig. 1.

how the basalt flows thin from several thousand metres thick near the Faeroe Islands (at 0 km in Fig. 15) to zero at the feather edge of the flows (at 220 km in Fig. 15). Although each profile was processed independently, the ties at the intersection point are good, giving confidence in our methodology.

We also show that there may be potential in using doubly mode-converted shear waves to give an extra possibility for imaging, although such studies are in their infancy. Converted *S*-wave imaging would benefit from ground-truthing using three-component seismometers on the seafloor to record shear waves directly, rather than relying on an additional conversion from *S* to *P* wave before the mode-converted arrivals can be imaged by a hydrophone streamer. Such an experiment combining long-offset streamer data with 90 four-component ocean-bottom seismometers was undertaken in summer 2002 along a 350 km profile crossing some of the FLARE profiles. Some cautionary comments are in order, however. Although the energy identified as being reflected from the base of the basalts produces a strong, high-amplitude arrival, since energy has been migrated over tens of thousands of metres laterally to produce these pre-stack depth-migrated images, any errors in the 2-D velocity model will translate into depth errors on the final PSDM image. Furthermore, any 3-D variations in the velocity field could also cause errors in migration, since we assume that only 2-D velocity variations occur along the line of the profile. The cusp in the base-basalt arrival at 160 km along the combined profile in Fig. 15 illustrates such an artefact caused by an insufficiently well-known velocity field. These limitations are, of course, true of any migrated profile. However, the large distances over which energy has been migrated mean that any small velocity errors are exacerbated in the depth migration and may translate into large apparent depth errors.

A further consideration that may cause depth errors in the migrated base-basalt image is that when the composite image is built the wide-angle base-basalt arrival is taken from a limited range of wide-angle offsets outside the water-wave cone. This has the advantage that the base-basalt arrivals are not contaminated by arrivals from shallower in the section or by multiples, and also that they are of high amplitude. However, the concomitant disadvantage is that there is no moderating control on the image from arrivals at near-normal offsets. We conclude that the best way to use the information from the wide-angle image is to make the best possible pre-stack depth migration of the entire data set (e.g. Fig. 13), using for the migration the improved velocity control produced by incorporating the long-offset arrivals, and then to use the composite wide-angle image as a guide to interpreting which reflections on the pre-stack depth migration image are from primary interfaces and which are from multiples. In this way the long-offset data with their good velocity control can be used to 'tag' specific arrivals as coming from the base-basalt or other deeper horizons, and thus to strengthen greatly the geological interpretation of the seismic profile.

Our technique of imaging below basalt flows is applicable in other cases of high-velocity layers obscuring imaging targets: salt (e.g. Gulf of Mexico), limestone and other high-velocity sedimentary rocks (e.g. Middle East).

ACKNOWLEDGMENTS

The data in this paper came from profiles shot by Western Geophysical and by Geco-Schlumberger as part of the Faeroes Large Aperture Research Experiment (FLARE), funded by Amerada Hess and its partners LASMO, Norsk Hydro and DOPAS. We thank all of the above for their support and for permission to use their data in this article. We are grateful to John Jones and Mirnal Sen for helpful reviews. Department of Earth Sciences, Cambridge contribution number 7364.

REFERENCES

Andersen, M.S., 1988. Late Cretaceous and early Tertiary extension and volcanism around the Faeroe Islands, in *Early Tertiary Volcanism and the Opening of the NE Atlantic*, Vol. 39, pp. 115–122, eds Morton, A.C. & Parson, L.M., Geological Society, London, Special Publication.

Barton, A.J. & White, R.S., 1997a. Crustal structure of the Edoras Bank continental margin and mantle thermal anomalies beneath the North Atlantic, *J. geophys. Res.,* **102,** 3109–3129.

Barton, A.J. & White, R.S., 1997b. Volcanism on the Rockall continental margin, *J. geol. Soc.,* **154,** 531–536.

Berthelsen, O., Noe-Nygaard, A. & Rasmussen, J., 1984. The deep drilling project 1980–1981 in the Faeroe Islands, *Ann. Societ. Scientar. Faeroensis, Suppl. IX,* Føroya Fródskaparfelag, Tórshavn.

Cowley, J., Jones, E., Jakubowicz, H., Williams, G. & Wombell, R., 1999. Results from a long offset experiment for sub-basalt imaging, *Am. Ass. Pet. Geol. Bull.,* **83,** 1307 (abstract).

Duindam, P. & Van Hoorn, B., 1987. Structural evolution of the West Shetland continental margin, in *Petroleum Geology of North West Europe,* pp. 765–773, eds Brooks, J. & Glennie, K.W., Graham & Trotman, London.

Earle, M.M., Jankowski, E.J. & Vann, I.R., 1989. Structural and stratigraphic evolution of the Faeroe–Shetland Channel and northern Rockall Trough, in *Extensional Tectonics and Stratigraphy of the North Atlantic Margins,* Vol. 46, pp. 461–469, eds Tankard, A.J. & Balkwill, H.E., Am. Ass. Petr. Geol. Mem.

Ebdon, C.C., Granger, P.J., Johnson, H.D. & Evans, A.M., 1995. Early Tertiary evolution and sequence stratigraphy of the Faeroe–Shetland Basin: implications for hydrocarbon prospectivity, in *The Tectonics, Sedimentation and Palaeoceanography of the North Atlantic Region,* Vol. 90, pp. 51–69, eds Scrutton, R.A., Stoker, M.S., Shimmield, G.B. & Tudhope, A.W., Geological Society, London, Special Publication.

Eldholm, O., *et al.*, 1989. Scientific results, sites 642–644, Norwegian Sea, *Proc. Ocean Drilling Program, Scientific Results,* 104, College Station, TX.

Fliedner, M.M. & White, R.S., 2001a. Sub-basalt imaging in the Faeroe–Shetland Basin with large-offset data, *First Break,* **19,** 247–252.

Fliedner, M.M. & White, R.S., 2001b. Seismic structure of basalt flows from surface seismic data, borehole measurements and synthetic seismogram modeling, *Geophysics,* **66,** 1925–1936.

Fruehn, J., Fliedner, M.M. & White, R.S., 2001. Integrated wide-angle and near-vertical incidence sub-basalt study using large aperture seismic data from the Faeroe–Shetland region, *Geophysics,* **66,** 1340–1348.

Hall, J. & Simmons, G., 1979. Seismic velocities of Lewisian metamorphic rocks at pressures to 8 kbar: relationship to crustal layering in north Britain, *Geophys. J. R. astr. Soc.,* **58,** 337–347.

Hinz, K., 1981. A hypothesis on terrestrial catastrophes: Wedges of very thick oceanward dipping layers beneath passive continental margins—their origin and paleoenvironmental significance, *Geol. Jahr. Reihe E,* **22,** 2–28.

Jolley, D.W., Clarke, B. & Kelley, S., 2002. Paleogene time scale miscalibration: evidence from dating of the North Atlantic igneous province, *Geology,* **30,** 7–10.

Jones, E.J.W., White, R.S., Hughes, V.J., Matthews, D.H. & Clayton, B.R., 1984. Crustal structure of the continental shelf off northwest Britain from two-ship seismic experiments, *Geophysics,* **49,** 1605–1621.

Kiørboe, L., 1999. Stratigraphic relationships of the Lower Tertiary of the Faeroe basalt plateau and the Faeroe–Shetland Basin, in *Petroleum Geology of Northwest Europe: Proc. 5th Conf.,* pp. 559–572, eds Fleet, A.J. & Boldy, S.A.R., Geological Society, London.

Kiørboe, L. & Petersen, S.A., 1995. Seismic investigation of the Faeroe basalts and their substratum, in *The Tectonics, Sedimentation and Palaeoceanography of the North Atlantic Region,* Vol. 90, pp. 111–124,

eds Scrutton, R.A., Stoker, M.A., Shimmield, G.A. & Tudhope, A.W. Geological Society, London, Special Publication.

Knox, R.W.O'B., Holloway, S., Kirby, G.A. & Baily, H.E., 1997. *Stratigraphic nomenclature of the UK North West Margin, 2. Early Paleogene Lithostratigraphy and Sequence Stratigraphy,* British Geological Survey, Nottingham.

Larsen, H.C. & Jakobsdóttir, S., 1988. Distribution, crustal properties and significance of seaward dipping subbasement reflectors off East Greenland, in *Early Tertiary Volcanism and the Opening of the NE Atlantic,* Vol. 39, pp. 95–114, eds Morton, A.C. & Parson, L.M., Geological Society, London, Special Publication.

Larsen, H.C., Dahl-Jensen, T. & Hopper, J.R., 1998. Crustal structure along the leg 152 drilling transect, in *Proc. Ocean Drilling Program,* Vol. 152, pp. 463–474, eds Saunders, A.D., Larsen, H.C. & Wise, S.W., Jr., Scientific Results, College Station, TX.

Larsen, H.C., Duncan, R.A., Allan, J.F. & Brooks, K., eds., 1999a. Scientific Results, sites 988–990, southeast Greenland margin, *Proc. Ocean Drilling Program,* Scientific Results, College Station, TX, Vol. 163.

Larsen, L.M. Waagstein, R., Pedersen, A.K. & Storey, M., 1999b. Trans-Atlantic correlation of the Palaeogene volcanic successions in the Faeroe Islands and East Greenland, *J. geol. Soc.,* **156,** 1081–1095.

Matthews, D.H. & Cheadle, M.J., 1986. Deep reflections from the Caledonides and Variscides west of Britain and comparison with the Himalayas, in *Reflection Seismology: a Global Perspective,* Vol. 13, pp. 5–19, eds Barazangi, M. & Brown, L., Am. Geophys. Union Geodynamics Series.

Mutter, J.C. & Zehnder, C.M., 1988. Deep crustal structure and magmatic processes: the inception of seafloor spreading in the Norwegian–Greenland sea, in *Early Tertiary Volcanism and the Opening of the NE Atlantic,* Vol. 39, pp. 35–48, eds Morton, A.C. & Parson, L.M., Geological Society London Special Publication.

Nielsen, P.H., Stéfansson, V. & Tulinius, H. 1984. Geophysical logs from Lopra-1 and Vestmanna-1, in *The Deep Drilling Project 1980–81 in the Faeroe Islands, Ann. Soc. Scient. Faeroensis,* **IX,** 115–136.

Ogilvie, J.S., Crompton, R. & Hardy, N.M., 2001. Characterization of volcanic units using detailed velocity analysis in the Atlantic Margin, West of Shetlands, United Kingdom, *Leading Edge,* **20,** 34–50.

Planke, S. & Eldholm, O., 1994. Seismic response and construction of seaward dipping reflectors in flood basalts: Vøring volcanic margin, *J. geophys. Res.,* **99,** 9263–9278.

Richardson, K.R., Smallwood, J.R., White, R.S., Snyder, D. & Maguire, P.K.H., 1998. Crustal structure beneath the Faroe Islands and the Faroe–Iceland Ridge, *Tectonophysics,* **300,** 159–180.

Richardson, K.R., White, R.S., England, R.W. & Fruehn, J., 1999. Crustal structure east of the Faroe Islands, *Petroleum Geosci.,* **5,** 161–172.

Ritchie, J.D., Gatliff, R.W. & Richards, P.C., 1999. Early Tertiary magmatism in the offshore NW UK margin and surrounds, in *Petroleum Geology of Northwest Europe: Proc. 5th Conf.,* pp. 573–584, eds Fleet, A.J. & Boldy, S.A.R., Geological Society, London.

Roberts, D.G., Backman, J., Morton, A.C., Murray, J.W. & Keene, J.B., 1984. Evolution of volcanic rifted margins: synthesis of Leg 81 results on the west margin of Rockall Plateau, *Initial Rep. Deep Sea Drill. Proj.,* **81,** 883–912.

Saunders, A.D., Fitton, J.G., Kerr, A.C., Norry, M.J. & Kent, R.W., 1997. The North Atlantic igneous province, in *Large Igneous Provinces; Continental, Oceanic and Planetary Flood Volcanism,* eds Mahoney, J.J. & Coffin, M.F., *Am. Geophys. Union, Geophys. Mon.,* **100,** 45–93.

Saunders, A.D., Larsen, H.C. & Wise, S.W., Jr., eds. 1998. Scientific Results, sites 914–919, East Greenland margin, *Proc. Ocean Drilling Program, Sci. Res.,* Vol. 152, Science Results, 152, College Station, TX.

Smallwood, J.R., White, R.S. & Staples, R.K., 1998. Deep crustal reflectors under Reydarfjördur, eastern Iceland: crustal accretion above the Iceland mantle plume, *Geophys. J. Int.* **134,** 277–290.

Smallwood, J.R., Towns, M.J. & White, R.S., 2001. The structure of the Faroe–Shetland Trough from integrated deep seismic and potential field modelling, *J. geol. Soc.,* **158,** 409–412.

Smythe, D.K., 1983. Faeroe–Shetland Escarpment and continental margin north of the Faeroes, in *Structure and Development of the Greenland–Scotland Ridge,* pp. 77–90, eds Bott, M.H.P., Saxov, S., Talwani, M. & Thiede, J., Plenum Press, New York.

Stoffa, P.L. & Buhl, P., 1979. Two-ship multichannel seismic experiments for deep crustal studies: expanding spread and constant offset profiles, *J. geophys. Res.,* **84,** 7645–7660.

Stoker, M.S., Hitchen, K. & Graham, C.C., 1993. *United Kingdom Offshore Regional Report: the Geology of the Hebrides and West Shetland Shelves, and Adjacent Deep-water Areas,* p. 149, HMSO, Norfolk.

Turner, J.D. & Scrutton, R.A., 1993. Subsidence patterns in western margin basins: evidence from the Faeroe–Shetland Basin, in *Petroleum Geology of Northwest Europe,* pp. 975–983, ed. Parker, J.R., Geological Society, London.

White, R. & Mckenzie, D., 1989. Magmatism at rift zones: the generation of volcanic continental margins and flood basalts, *J. geophys. Res.,* **94,** 7685–7729.

White, R.S. & Stephen R.A., 1980. Compressional to shear wave conversion in oceanic crust, *Geophys. J. R. astr. Soc.,* **63,** 547–566.

White, R.S., Fruehn, J., Richardson, K.R., Cullen, E., Kirk, W., Smallwood, J.R. & Latkiewicz, C., 1999. Faroes Large Aperture Research Experiment (FLARE): imaging through basalts, in *Petroleum Geology of Northwest Europe: Proc. 5th Conf.,* pp. 1243–1252, eds Fleet, A.J. & Boldy, S.A.R., Geological Society London.

Zelt, C.A. & Smith, R.B., 1992. Seismic traveltime inversion for 2-D crustal velocity structure, *Geophys. J. Int.* **108,** 16–34.